The Effect of Diffusion on the Hydrotreatment of n-C16: A Novel Method to Calculate the Weisz-Prater Number

Junhao Sun, Chao Mu, Yi Li, Yujun Zhao, Shengping Wang[*], Xinbin Ma

Key Laboratory for Green Chemical Technology,

School of Chemical Engineering and Technology, Tianjin University,

Collaborative Innovation Center of Chemical Science and Engineering (Tianjin),

Tianjin 300072, China

Abstract

Weisz-Prater number (N_{W-P}) is often applied to assess the internal diffusion effect in heterogeneous catalytic reactions. However, the traditional calculation method with excessive empirical reference values affects the accuracy remarkably. A series of Pt/HPMo/SBA-15 catalysts with the pore size as a single variable were prepared to calculate the N_{W-P} with a developed model combining the diffusion-reaction kinetic method. Utilizing dimensionless variables, internal effectiveness factor (η) and Thiele modulus (Φ_n), and the apparent activities over catalysts with different diffusion capacity, N_{W-P} is obtained with improved accuracy. For the diffusion effect on the hydrotreatment of n-C16, according to the more precise N_{W-P}, the pore size should be not less than 10 nm to avoid the step-limitation of internal diffusion in the premise of adequate acid sites. Using the novel method, a conclusion is drawn that the formation of m-i-C16 is more susceptible to internal diffusion than the consumption of n-C16.

Keywords: Weisz-Prater number; diffusion-reaction kinetics; hydrocracking

1. Introduction

High demand for jet fuel and a shortage of oil resources have attracted researchers to visit some processes of biological transformation[1-4]. In the two-stage hydrogenation route which includes the step of vegetable oil or animal fat hydrotreating and the followed step of hydrocracking, the isomerization and selective cracking of long-chain alkanes is the key process to meet the requirements of molecular weight and freezing point[5-8]. In consequence, the selectivity to the target product jet fuel and the ratio of iso-alkanes to n-alkanes are the important indicators. Hence, the most suitable catalyst for hydrocracking of long-chain alkanes to produce jet fuel is the one with strong isomerization and weak cracking capacity, which is reported in the previous work of our group[9]. In light of this strategy, to design the most suitable catalyst, it is necessary to obtain clues about the relationship between the selectivity to the target products jet fuel and the microscopic characteristics, such as the acid property, bifunctional activity sites intimacy, and the mass transferability of the catalyst. To this end, further research about not only activity sites but also the diffusion effect is needed.

It is now well established and can't be disputed that the rate-limiting step in the hydrotreatment of long-chain alkanes is the isomerization and cracking of the alkyl carbonium ions on the Brønsted acid sites[10] and the selectivity to the product is subject to the adsorption energetics and diffusion of primarily formed product[11]. Therefore, too strong adsorption of the primarily formed product affects adversely the

selectivity to the subsequent product by favoring over cracking. Besides, the degree of branching is closely related to the pore structure of the catalyst[12, 13]. Comparing to microporous zeolites, such as ZSM-5, Y, or BETA, ordered mesoporous materials with weak acid sites are favorable for restraining secondary cracking and enhancing the degree of branching[14].

The selectivity shift phenomenon over catalysts with different pore structure can be attributed to an enhanced mass transfer and faster desorption of the primary product, due to a shorter diffusion path, which depends on the molecular dimension and pore size of the catalyst[15]. Remarkably, there are several isomers of n-C16 with larger dynamic dimensions in the hydrotreatment of n-C16. It is of great significance to rule out the intraparticle diffusion limitation by investigating the effect of pore size on the hydrotreatment of n-C16.

The Weisz-Prater number is often applied to assess the internal diffusion effect in heterogeneous catalytic reactions[16]. It's a dimensionless number that compares the rate of reaction with the rate of mass transfer in the pores. The values of most physical quantities can be measured experimentally except the effective diffusion coefficient D_{eff} which is associated with the tortuosity factor τ of the catalyst. As a ratio of the actual distance that the molecule diffuses to the shortest distance between any two points on the surface of the catalyst, the tortuosity τ is ever-changing because there are many random and irregular channels inside the catalyst[17, 18], making it difficult to obtain the accurate values of the tortuosity. For the same catalyst, the empirical value

of τ in different literatures is even several times different[19-22], which is the main source of error undoubtedly.

Another classic method for investigating the effects of diffusion is the diffusion-reaction kinetic method. By shrinking the size of catalyst particles at a constant space velocity, the intrinsic reaction rate can be obtained[23]. However, the practical feasibility of this method is non-ideal because the larger drop of bed pressure resulted from the smaller catalyst particle size will lead to the back-mixing of the product, causing the uncontrolled product distribution. All in all, a more efficient method to calculate N_{W-P} needs to be developed for diffusion research not only in the hydrotreatment of long-chain alkanes but also in other heterogeneous catalytic systems with macromolecules as reactants.

Herein, a series of Pt/HPMo/SBA-15 catalysts with the pore size as a single variable was prepared to catalyze the hydrocracking and isomerization of n-C16. The diversity of diffusion performance over different catalysts was characterized by TG-TPD of n-C16 and Zero-Length Column (ZLC) of n-C8. Based on the apparent reaction rate of n-C16 over catalysts with different pore size and particle diameter, a novel mathematical model is developed to calculate the Weisz-Prater number, which can avoid the adverse effect caused by excessive bed lamination and improve the accuracy with fewer empirical formulas. Further, the effect of pore size on the selective hydrocracking and isomerization of n-C16 to produce jet fuel was studied via the novel model.

2. Experiment

2.1. Catalyst preparation

The ordered mesoporous supports SBA-15 with different pore sizes were prepared as similar conditions except for the crystallization temperature. 2 M HCl (Tianjin Kemiou Chemical Reagent Co., Ltd., China) solutions were prepared in advance and reserved. For the previous steps, the three samples were exactly the same. 10 g P123 (average Mn ≈ 5800 , ENZO) was mixed with 350 ml HCl solution and stirred well at 35°C until a clear solution was obtained. Then, 21 g TEOS (Tianjin Kemiou Chemical Reagent Co., Ltd., China) was added drop by drop. The solution continues to be stirred for 24 h. The first sample was stirred for an additional 24 h, for a total of 48 h. The remaining two samples were transferred into a 1 L stainless steel autoclave lined with polytetrafluorethylene (PTFE) and kept in an oven for 24 h. The crystallization temperature of the second sample is 100 °C while that of the third one is 130 °C. After crystallization, all samples were filtrated and washed. Finally, the samples were dried at 80 °C for 12 h and calcinated at 550 °C for 5 h. The ultima supports were named as SBA-15-n, while the symbol "n" represents the pore size in nanometers.

The next step to load the phosphomolybdic acid (HPMo, 35 wt. %) and platinum (Pt, 0.5 wt. %) was followed by the method in the previous work[9]. The series of catalysts with the pore size as a single variable was named Pt/HPMo/SBA-15-n after loading the active ingredient.

2.2. Catalyst characterization

On the ASAP-2020 instrument (Micromeritics, USA), three carriers were measured for their pore structure by N_2 physisorption after the degas pretreatment at 300 °C for 4 h. The specific surface area of each carrier was calculated through the Brunauer-Emmett-Teller (BET) equation while the size distribution of mesopores and pore volume of samples were determined by the Barrett-Joyner-Halenda (BJH) method.

X-ray diffraction (XRD) results were recorded on a Rigaku D/max-2500 diffractometer equipping Cu Kαradiation (λ=0.154 nm). The carriers were scanned from 0.5 ° to 5 ° at the rate of 0.5 °/min to character the structure of SBA-15 and the catalysts were scanned from 8° to 80° at the rate of 10°/min to characterize the dispersed state of HPMo.

The Nicolet 6700 (Thermo Fisher, USA) instrument employing an in-situ cell with a vacuum system was used for recording the IR spectra of adsorbed pyridine. About 15 mg sample was pressed into a 13mm self-supporting wafer. Before pyridine adsorption, the wafer was pretreated for 2 h at 350 °C. Thereafter the background spectrum of the wafer was recorded at 150 °C. The sample was adsorbed to a saturated state by pyridine, and then vacuumed for 30 minutes to remove the physically adsorbed pyridine. Finally, the spectra were collected to determine the amount of Brønsted and Lewis acids in the range of 650–4000 cm^{-1}.

The acid strength of catalysts was measured through the temperature-programmed desorption of NH_3 (NH_3-TPD) experiment using the Auto chem II 2920 chemical

adsorption instrument (Micromeritics, USA). To remove the adsorbed impurities and reduce the metal Pt, about 100 mg catalyst (40-60 mesh) was pretreated for 2 h under 10% H_2/Ar at 350 °C. After the temperature dropped to 100 °C, 10% NH_3/He was passed through the catalyst at a flow rate of 20 ml/min for 1 h. After the physically adsorbed NH_3 was removed, the desorbed NH_3 was detected by mass spectrometry (MS) with the temperature range from 100°C to 650 °C at a rate of 10 °C/min.

CO chemisorption was carried out on the same adsorption instrument to characterize the number of Pt atoms exposed on the catalyst surface. About 50 mg catalyst (40-60 mesh) was reduced at 350 °C for 2 h under 10% H_2/Ar. After the temperature was lowered to 50 °C, the pulse adsorption with 10% CO/He was performed. The adsorption ended after the pulse signal was stable.

Using the STA-449F3 thermal gravimetric analyzer (Netzsch, Germany), thermal gravimetric temperature-programmed desorption (TG-TPD) of n-C16 was performed. Before the test, the sample (≈5 mg) was reduced in the reactor, and then n-C16 was adsorbed to a saturated state under a nitrogen purge at 300 °C. As N_2 was shielding gas and air was purge gas, the sample was heated to 500 °C at the rate of 10°C/min to compare the desorption variation of n-C16 over different catalysts.

2.3. ZLC method

The ZLC method was proposed by Eic and Ruthven to measure intracrystalline diffusivities[24]. It was assumed that the desorption is rate-controlled entirely by diffusion over the particle, maintaining equilibrium with the surrounding fluid at the

external surface[25].

As shown in Fig. 1, the experimental set-up consists of three sections: the gas preparation section, the ZLC unit, and the detector. In a typical run, a small amount of sample ($\approx$5mg, 40-60 mesh) was loaded inside of the ZLC unit with a thin flake in shape. Before the experiment, the sample was heated to 350 °C and purged with pure N_2 steam at 60 ml/min for 2 h to remove any moisture or any impurity. After the temperature dropped to 130 °C, the bed of the catalyst was saturated with the model sorbate, n-C8 in the N_2 carrier via the saturated evaporation tank at an inverse status of the 4-way valve. Backing to the purge situation, at time zero, pure N_2 was used to purge the ZLC unit and the resulting desorption signal was collected by FID, as a function of time.

The relative gas concentration (c/c_0) is given by the following equation[26, 27]:

$$\frac{c}{c_0} = \sum_{n=1}^{\infty} \frac{2L}{\beta_n^2 + L(L+1)} \exp(\frac{-\beta_n^2 D_e t}{R^2}) ------(1)$$

$$\beta_n \cot \beta_n + L - 1 = 0 ------(2)$$

$$L = \frac{1}{3} \frac{F}{K V_S} \frac{R^2}{D_e} ------(3)$$

Where β_n and L are given by the roots of the auxiliary equation:

Where F is the purge flow rate, V_s is the sample volume, K is the dimensionless Henry's Law constant, and D_e is the effective diffusivity.

The effective diffusion time constant (D_e/R^2) could be determined by fitting

equations (1)-(3) with the experimental ZLC data using the Matlab software in the complete time range[28, 29].

2.4. Catalyst testing

The hydrotreatment of n-C16 was carried out on a fixed-bed reactor. In a typical test, 0.113g catalyst (40-60 mesh) was placed in the isothermal zone of the reaction tube, subsequently online reduced in pure hydrogen at350 °C for 2 h. Thereafter the reactor was cooled down to 340 °C and then the liquid raw material of n-C16 in a buffer tank passed through the reaction tube through a pump at a flow rate of 0.02 ml/min (WHSV=8 h^{-1}). After 6 h of stabilization time, the liquid product was collected every 2 hours.

The components of the product are analyzed by GC (SP-2100GC, PC-PONA). Following our previous work[9], the product is divided into <C9 (gasoline), C9-C14 (jet fuel), s-i-C16 (the single-branched isomer of C16), and m-i-C16 (the multi-branched isomer of C16).

3. Results and discussion

3.1. Textural and chemical properties of Pt/HPMo/SBA-15-n

Fig. 2, Fig. 3, and Table 1 are the textural properties of carriers. The nitrogen adsorption-desorption isotherms of each sample show a type IV curve and the hysteresis ring gradually shift towards high pressure which illustrates that each carrier possesses mesoporous distribution and the pore diameter gradually increases. The

characteristic diffraction peaks of (100) crystal face in Fig. 3 (a) indicate that all carriers own hexagonal mesoporous stricture which is long-range and high crystallinity[30]. According to the approximate integer value of the calculated aperture in Table 1, three carriers were named as SBA-15-n (n=5, 7, 10). Besides, as shown in Fig. 3 (b), there is no obvious diffraction peak of bulk HPMo after loading, which proves that the HPMo is uniformly dispersed on each carrier.

Fig. 4 and Table 2 are the chemical properties of Pt/HPMo/SBA-15-n. From the MS signal of NH_3 during the TPD process in Fig. 4 (a), there is no significant discrepancy in the acid strength of three catalysts. There is only one kind of weak acid. As for the number of acid sites, three catalysts are roughly the same no matter Brønsted or Lewis acid, which is displayed in Fig. 4 (b) and Table 2. After CO chemisorption measurement, the ratio of accessible Pt to Brønsted acid sites is listed in Table 2. The ratio of all catalysts is great than 0.03 indicating that the metal active sites are sufficient, in other words, the hydrotreatment of n-C16 is not limited by the step of hydrogenation or dehydrogenation[31].

In brief, the physical and chemical properties of three catalysts are similar except for the pore size. Scilicet, a series of catalysts with the pore size as a single variable were successfully prepared. In the tentative evaluation of catalysts, a significant difference in the conversion of n-C16 emerged in the identical condition. Therefore, the essential causes of the differences are thoroughly studied in the next.

3.2. Mass transfer performance of Pt/HPMo/SBA-15-n

TPD measurement of the reactant molecule can present the difference of performance in the adsorption and diffusion of the catalyst. In this work, the boiling point of the reactant molecule, n-C16, is too high, which makes it difficult to collect the TCD signal. To overcome this difficulty, TGA and TPD were combined for testing. After pretreatment, the saturated catalyst adsorbed with n-C16 was used for TG analysis in an inert atmosphere from 100 °C to 500 °C. The upper limit of the test temperature is lower than that of the conventional TG analysis in order to avoid the thermal cracking reaction of n-C16. It can be seen from Fig. 5 that the adsorbate is gradually desorbed with increasing temperature as impurities and water have been removed during the pretreatment. The weight loss rate over Pt/HPMo/SBA-15-10 is significantly faster than that of the other two catalysts, which can be caused by the influence of the individual pore size on the diffusion of the desorbing n-C16 molecules[32]. The important premise for this explanation is that in many cases the chemical reaction and the diffusion rate are slow as compared to the adsorption-desorption events[33].

ZLC method was used for the semi-quantitative test of the catalyst's diffusion performance. By modifying the temperature of recirculation cooling water, the concentration of adsorbate, n-C8, at the ZLC unit was maintained at a low level (no more than 0.025 bar)[26] to make sure that the measurement was carried out within the linear region of the adsorption isotherm (Henry's law region) as required by the ZLC

theory[34]. Before formal measurement, some verification experiments over Pt/HPMo/ SBA-15-5 were conducted to ensure that the experimental conditions meet the other theoretical requirements. As presented in Fig. 6 (a), the comparison between the blank run and the experimental run was used to examine the effect of the dead volume in the ZLC device. It took about 14 minutes to purge the relative concentration of n-C8 in the catalyst bed from 1 to 0.01 at a nitrogen rate of 60 ml/min, under 130 °C while it only spent about 1.6 minutes for the blank run without catalyst under the identical condition. The difference in desorption time is nearly ten times, indicating that the effect of the dead volume in the ZLC device can be ignored. Fig. 6 (b) and Fig. 6 (c) are both desorption curves of n-C8 with different carrier gas flow rates over Pt/HPMo/SBA-15-5 at 130 °C while the latter is a partially enlarged view of the former during the post-desorption period. With the extension of the time, the desorption speed gradually decreased. As the desorption flow rate increases, the time it takes for the relative concentration to decrease from 1 to 0.01 becomes shorter and shorter and the curve in the later stage of desorption gradually becomes parallel, which means that the desorption process is gradually controlled by internal diffusion instead of external diffusion. As shown in Fig. 6 (d), the effective diffusion time constant (D_e/R^2) at different flow rates was determined by fitting the experimental ZLC data using the Matlab software in the complete time range. The effective diffusion time constant (D_e/R^2) first increases and then stabilizes with the increase of the desorption flow rate. When the desorption flow rate is greater than 100 ml/min,

the constant (D_e/R^2) is stable, indicating that the desorption process is controlled by internal diffusion[35], so the others can be measured at a flow rate of 100 ml/min.

Desorption curves over different catalysts are presented in Fig. 7 with corresponded effective diffusion time constant (D_e/R^2). Under the same desorption conditions, the larger the pore size of the catalyst, the faster the desorption rate, and the larger the constant (D_e/R^2), which is consistent with the result of n-C16-TG-TPD.

Through qualitative analysis of n-C16-TG-TPD and semi-quantitative analysis of ZLC, it is found that there is a significant difference in the diffusion performance of catalysts with different pore sizes, which may be the main reason for the activity discrepancy. It is well known that the difference in diffusion performance will affect the activity, but whether it will become a speed control step requires further in-depth discussion.

3.3. A novel mathematical model to calculate the Weisz-Prater number

Weisz-Prater number (N_{W-P}) is particularly useful to evaluate the influence of pore diffusion on a catalytic reaction because it provides a dimensionless number containing only observable parameters that can be readily measured or calculated. For the first-order reaction, when N_{W-P} is less than 0.6, the internal diffusion may be neglected and larger N_{W-P} implies more influence of diffusion[16, 36, 37].

Weisz-Prater number is given as follows[38]:

$$N_{W-P} = \frac{\text{apparent reaction rate}}{\text{internal diffusion rate}} = \frac{r_a * \rho_c * R^2}{D_e * C_{AS}} - - - - - (4)$$

where r_a (mol/(gcat*s)) is the apparent reaction rate. ρ_c (kg/m^3) is the density of the catalyst. R (m) is the radius of the catalyst particle. C_{AS} (mol/m^3) is the concentration of species at the external surface of catalysts, and D_e (m^2/s) is the effective diffusion coefficient which is usually calculated by Eq. (5).

In this important formula, porosity (ε) can be easily measured. The limiting factor (

$$D_e = \frac{\varepsilon \sigma}{\tau} D_P ------(5)$$

σ) is a function of the ratio of the cross-sectional area of the largest pore to the smallest pore in the catalyst (A_2/A_1)[39]. The pore size distribution of conventional catalysts is wide, and the uncertainty of the area ratio (A_2/A_1) leads to the accurate determination of the limiting factor (σ) being hindered. As mentioned in the introduction, the tortuosity factor (τ) is a ratio of the actual distance that the molecule diffuses to the shortest distance between any two points on the surface of the catalyst, which is ever-changing because there are many random and irregular channels inside the catalyst[17]. For the same catalyst, different empirical values of the tortuosity τ have been put forward by the previous papers, the gap between which is particularly large[40-43], reducing the credibility of the data undoubtedly. As for the diffusion coefficient in the pores (D_p), it can also be derived from many empirical formulas, considering molecular diffusion, Knudsen diffusion, and intractytalline diffusion, which won't be described in detail here. Generally, the diversity of catalyst pores

leads to low accuracy of N_{W-P} based on solely theoretical calculations and it's

necessary to combinate the experimental data with the diffusion-reaction kinetics

method.

By introducing the rate of intrinsic reaction, Eq. 6 can be transformed from Eq. 4 as

follows:

$$\frac{r_a * \rho_c * R^2}{D_e * C_{AS}} = \frac{\text{apparent reaction rate}}{\text{internal diffusion rate}}$$

$$= \frac{\text{apparent reaction rate}}{\text{instrinsic reaction rate}} * \frac{\text{instrinsic reaction rate}}{\text{internal diffusion rate}} - - - - - -(6)$$

$$\frac{r_a * \rho_c * R^2}{D_e * C_{AS}} = \eta * \Phi_1^2 = 3(\Phi_1 * \coth \Phi_1 - 1) - - - - - -(7)$$

According to the concept of two dimensionless variables, internal effectiveness

factor (η) and Thiele modulus (Φ_n(where 'n' is the reaction order)), Eq. 6 can be

transformed into Eq. 7 based on the first-order reaction[44].

If catalytic evaluation were made under identical conditions with different radius of

the catalyst particle, for example, R_1 and R_2, whose apparent reaction rate

corresponding to r_{a1} and r_{a2} could be easily measured. The radius can be in a suitable

range to avoid an excessive drop in bed pressure. Then, we will apply for Eq. 7 of

runs 1 and runs 2 and take the ratio to obtain Eq. 8.

The parameters ρ_c, D_e and $C_{AS}^{\square}$ were canceled because the runs were carried out

$$\frac{r_{a1} * R_1^2}{r_{a2} * R_2^2} = \frac{\Phi_{11} * \coth \Phi_{11} - 1}{\Phi_{12} * \coth \Phi_{12} - 1} - - - - - -(8)$$

under identical conditions. For first-order irreversible reactions over spherical

$$\Phi_1^2 = \frac{r_i * \rho_c * R^2}{D_e * C_{AS}} - - - - - -(9)$$

catalysts, the Thiele modulus is[45]:

where r_i (mol/(gcat*s)) is the intrinsic reaction rate. Taking the ratio of the Thiele

modulus for runs 1 and runs 2, we will obtain Eq. 10.

Combining Eq. 8 and Eq. 10, from the known r_{a1}, r_{a2}, R_1, R_2, we can get the value of

$$\frac{\Phi_{11}}{\Phi_{12}} = \frac{R_1}{R_2} - - - - - - (10)$$

Φ_{11} and Φ_{12}. Letting the subscript 0 refer to the theoretical state where the internal

diffusion control was virtually eliminated (say, η=0.95). Next, according to the Eq. 7

and Eq. 10, we can get Φ_{10} and R_0. Finally, based on Eq. 8 and the known Φ_{10}, R_1, and

Φ_{11}, r_{a1}, R_1 or Φ_{12}, r_{a2}, R_2, the important variable r_{a0}, that is the intrinsic reaction rate

(r_i) will be obtained. For different runs over the same catalyst, based on Eq. 7 and Eq.

6 with the same intrinsic reaction rate measured before, the internal effectiveness

factor (η), Thiele modulus (Φ_1) and then the N_{W-P} will be accurately derived. To make

the model clearer, the flow of the calculations is shown in Fig. 8.

3.4. The effect of pore size on the hydrocracking and isomerization of n-C16

The hydrocracking and isomerization of n-C16 were carried out over each catalyst

with different diameter of the catalyst particle, specifically, dp=0.675 mm (20-40

mesh) and dp=0.375 mm (40-60 mesh). The apparent reaction rate over each catalyst

with different diameters and the intrinsic reaction rate calculated in the novel method

was present in Fig. 9. As for Fig. 9 (a), no matter the diameter of the catalyst particle,

the apparent consumption rate of n-C16 is positively related to the pore size of the

catalyst. There is a common phenomenon for each catalyst is that the larger the particle diameter, the lower the reaction rate. In the structural properties of the catalyst, the pore size and particle diameter will significantly affect the diffusion rate. No matter to increase the pore size or reduce the particle diameter, it can weaken the effect of internal diffusion. For catalysts with the same pore size, combining the novel calculation method with the apparent reaction rate under different particle sizes, the intrinsic reaction rate when the internal diffusion is completely eliminated can be calculated. As shown in Fig. 9 (a) and (b), it is clearly noted that the derived value of the intrinsic reaction rate over the catalysts with the different pore sizes but similar active site properties are almost consistent. In other words, the intrinsic reaction rate is irrelevant to the pore size of the catalysts. Since the molecule with the largest kinetic diameter in the reaction is m-i-C16, further analysis was performed regarding the formation rate of m-i-C16. Except that the ordinate is changed, the other chart element and data analysis results in Fig. 9 (b) are the same as that in Fig. 9 (a).

It is important to mention that for the same run of catalytic evaluation, the formation rate of m-i-C16 is much smaller than the consumption rate of n-C16, that is, when the hydrotreatment of n-C16 is affected by internal diffusion, in specific analysis, the generation process of m-i-C16 will be speed-limiting.

Based on the novel method, from the known reaction rate, the Weisz-Prater numbers were listed in Table 3. For the catalysts with different pore sizes, the numbers were obtained from the different particle diameter and different original reaction rates. The

d_{p0} is the theoretical value of particle diameter when the internal diffusion is virtually eliminated. Looking down from the first line of the table, no matter the basis d_p and reaction rate, the d_{p0} is positively correlated with the pore size while N_{W-P} is negatively correlated with the pore size. The method of increasing the pore size can availably weaken the effect of internal diffusion and reduce the size requirements for the catalyst particle diameter. For the same catalyst based on the uniform reaction rate, no matter the consumption of n-C16 or the formation of m-i-C16, the smaller the d_p, the smaller the N_{W-P}. In addition to expanding the pore size, reducing the particle diameter can also effectively weaken the effect of internal diffusion. As for the identical catalyst, N_{W-P} calculated based on the formation rate of m-i-C16 is larger than that based on the consumption rate of n-C16, indicating that the formation of m-i-C16 is more sensitive to the diffusion effect. That is, to determine whether the reaction is controlled by internal diffusion, the N_{W-P} calculated based on the formation rate of m-i-C16 is more convincing.

As mentioned previously, for the first-order reaction, when N_{W-P} is less than 0.6, the internal diffusion may be neglected and larger N_{W-P} implies more influence of diffusion. Since the proportion of hydrogen is greatly excessive, a pseudo-first-order reaction for the hydrocracking of n-C16 is assumed. From the special values, it can be observed that the internal diffusion has a significant influence on the hydrocracking and isomerization of n-C16 when the particle diameter is 0.675 mm (20-40 mesh) or the pore size is 5 nm since the N_{W-P} are much higher than 0.6. For Pt/HPMo/SBA-15-7

with smaller particle diameter (0.375 mm), the N_{W-P} calculated based on the consumption rate of n-C16 is smaller than 0.6 but the N_{W-P} calculated based on the formation rate of m-i-C16 is larger than 0.6. In other words, the hydrocracking and isomerization of n-C16 over Pt/HPMo/SBA-15-7 is also controlled by the internal diffusion effect of m-i-C16 but not n-C16. As for the catalyst Pt/HPMo/SBA-15-10 with a particle diameter of 0.375 mm (40-60 mesh), no matter the calculation basis of the reaction rate, the N_{W-P} is always below 0.6, which signifies that under the model conditions, the internal diffusion effect of hydrocracking and isomerization of n-C16 over Pt/HPMo/SBA-15-10 with an average pore size in 10 nm is virtually eliminated. To go further, in the hydrocracking and isomerization of n-C16, the distribution of products is influenced by the superposition of metal properties, acid nature, and diffusion performance. Taking advantage of this novel method, the more precise N_{W-P} can be acquired to clear the contribution degree of diffusion performance.

4. Conclusion

In this work, a series of Pt/HPMo/SBA-15-n catalysts with the pore size as a single variable were successfully prepared and the difference of diffusion performance was characterized by TG-TPD of n-C16 and ZLC of n-C8. The product distribution is influenced greatly by pore size in the hydrotreatment of n-C16. For a more precise quantitative discussion of diffusion, utilizing two dimensionless variables, internal effectiveness factor (η) and Thiele modulus (Φ_n), and the apparent reaction rate over

catalysts with different pore size and particle diameter, a novel mathematical method

is developed to calculate the Weisz-Prater number, which can reduce the error caused

by the empirical formula and excessive drop of bed pressure. Using the novel method,

a conclusion is drawn that the pore with a large size is more favorable for the

hydrocracking and isomerization of n-C16 and the formation of m-i-C16 is more

susceptible to the internal diffusion than the consumption of n-C16 in the

hydrotreatment of n-C16 to produce jet fuel. On the condition of having sufficient

metal sites and the density of the acid sites being about 300 μmol/g, the pore size of

the catalyst should be not less than 10nm to ensure that the reaction is not limited by

internal diffusion. The provided novel method to calculate the N_{W-P} can be extended to

other heterogeneous catalytic systems with macromolecules as reactants to discuss the

diffusion effect and design the catalyst more accurately.

Acknowledgments

References

[1]   Huber G W, Iborra S, Corma A. Synthesis of transportation fuels from biomass:

Chemistry, catalysts, and engineering[J]. Chem Rev, 2006,106(9):4044-4098.

[2]   Murata K, Liu Y, Watanabe M M, et al. Hydrocracking of algae oil into aviation

fuel-range hydrocarbons using a Pt-Re catalyst[J]. Energ Fuel, 2014,28(11):6999-7006.

[3] Karatzos S, van Dyk J S, McMillan J D, et al. Drop-in biofuel production via conventional (lipid/fatty acid) and advanced (biomass) routes. Part I[J]. Biofuel Bioprod Biore, 2017,11(2):344-362.

[4] Eller Z, Varga Z, Hancsok J. Advanced production process of jet fuel components from technical grade coconut oil with special hydrocracking[J]. Fuel, 2016,182:713-720.

[5] Kim M Y, Kim J, Lee M, et al. Maximizing biojet fuel production from triglyceride: Importance of the hydrocracking catalyst and separate deoxygenation/hydrocracking steps[J]. ACS Catal, 2017,7(9):6256-6267.

[6] Baroutian S, Aroua M K, Raman A A A, et al. Blended aviation biofuel from esterified Jatropha curcas and waste vegetable oils[J]. J Taiwan Inst Chem E, 2013,44(6):911-916.

[7] Zhang M, Wang L, Chen Y, et al. Creating mesopores in ZSM-48 zeolite by alkali treatment: Enhanced catalyst for hydroisomerization of hexadecane[J]. J Energy Chem, 2016,25(3):539-544.

[8] Mendes P S F, Silva J M, Ribeiro M F, et al. Quantification of metal-acid balance in hydroisomerization catalysts: A step further toward catalyst design[J]. AIChE J, 2017,63(7):2864-2875.

[9] Sun J, Li Y, Mu C, et al. Supported heteropolyacids catalysts for the selective hydrocracking and isomerization of n-C16 to produce jet fuel[J]. Appl Catal A:

Gen, 2020,598:117556.

[10] Coonradt H L, Garwood W E. Briefs-"mechanism of hydrocracking. Reactions of paraffins and olefins"[J]. Ind Eng Chem Process Des Dev, 1964,56(1):69.

[11] Kenmogne R, Finiels A, Cammarano C, et al. Hydroconversion of n-hexadecane over bifunctional microporous and mesoporous model catalysts. Influence of pore architecture on selectivity[J]. J Catal, 2015,329:348-354.

[12] Soualah A, Lemberton J L, Pinard L, et al. Hydroisomerization of long-chain n-alkanes on bifunctional Pt/zeolite catalysts: Effect of the zeolite structure on the product selectivity and on the reaction mechanism[J]. Appl Catal A: Gen, 2008,336(1-2):23-28.

[13] Triwahyono S, Jalil A A, Izan S M, et al. Isomerization of linear C5-C7 over Pt loaded on protonated fibrous silica@Y zeolite (Pt/HSi@Y) [J]. J Energy Chem, 2019,37:163-171.

[14] Park K, Ihm S. Comparison of Pt/zeolite catalysts for n-hexadecane hydroisomerization[J]. Appl Catal A: Gen, 2000,203(2):201-209.

[15] Heeribout L, Vincent R, Batamack P, et al. Brønsted acidity of amorphous silica-aluminas studied by 1H NMR[J]. Catal Lett, 1998,53(1-2):23-31.

[16] Vannice M A. Kinetics of catalytic reactions[M]. Springer, 2005.

[17] Scott H, Fogler. Elements of chemical reaction engineering[M]. New Jersey: Prentice-Hall Inc, 2006.

[18] Ramírez E, Larrayoz M A, Recasens F. Intraparticle diffusion mechanisms in SC sunflower oil hydrogenation on Pd[J]. AIChE J, 2006,52(4):1539-1553.

[19] Gang W, Chen Z T, Lan X Y, et al. Restricted diffusion of residual molecules in catalyst pores under reactive conditions[J]. Chem Eng Sci, 2011,66(6):1200-1211.

[20] Ming C T, Chen Y W, Li C. Restrictive diffusion under hydrotreating reactions of heavy residue oils in a trickle bed reactor[J]. Ind Eng Chem Res, 1993,32(8):1603-1609.

[21] Tsai C H, Massoth F E, Lee S Y, et al. Effects of solvent and solute configuration on restrictive diffusion in hydrotreating catalysts[J]. Ind Eng Chem Res, 1991,30(1):22-28.

[22] Ware R A, Wei J. Catalytic hydrodemetalation of nickel porphyrins II. Effects of pyridine and of sulfiding[J]. J Catal, 1985,93(1):122-134.

[23] Chen A C, Chen S L, Hua D, et al. Diffusion of heavy oil in well-defined and uniform pore-structure catalyst under hydrodemetallization reaction conditions[J]. Chem Eng J, 2013,231:420-426.

[24] Eic M, Ruthven D M. A new experimental technique for measurement of intracrystalline diffusivity[J]. Zeolites, 1988,8(1):40-45.

[25] Ruthven D M, Vidoni A. ZLC diffusion measurements: Combined effect of surface resistance and internal diffusion[J]. Chem Eng Sci, 2012,71:1-4.

[26] Gelles T, Lawson S, Thakkar H, et al. Diffusion kinetics of ethane, ethylene, and their binary mixtures in ethane-selective adsorbents[J]. Sep Purif Technol, 2020,230(115872).

[27] Shirani B, Han X, Eic M. Application of ZLC technique for a comprehensive

study of hydrocarbons' kinetics in carbon molecular sieves and zeolites[J]. Sep Purif Technol, 2020,230(115831).

[28] Brandani S. Analytical solution for ZLC desorption curves with bi-porous adsorbent particles[J]. Chem Eng Sci, 1996,51(12):3283-3288.

[29] Hoang V T, Huang Q, Malekian A, et al. Diffusion characterization of a novel mesoporous zeolitic material[J]. Adsorption, 2005,11(1):421-426.

[30] Tang H, Lan G, Zhong J, et al. Easy synthesis of iron doped ordered mesoporous carbon with tunable pore size[J]. J Nat Gas Chem, 2012(21):275-281.

[31] Alvarez F, Ribeiro F R, Perot G, et al. Hydroisomerization and hydrocracking of alkanes 7. Influence of the balance between acid and hydrogenating functions on the transformation of n-decane on PtHY catalysts[J]. J Catal, 1996,162:179-189.

[32] Meriaudeau P, Tuan V A, Nghiem V T, et al. SAPO-11, SAPO-31, and SAPO-41 molecular sieves: Synthesis, characterization, and catalytic properties in n-octane hydroisomerization[J]. J Catal, 1997.

[33] Bidabehere C M, García J R, Sedran U. Transient effectiveness factor. Simultaneous determination of kinetic, diffusion and adsorption equilibrium parameters in porous catalyst particles under diffusion control conditions[J]. Chem Eng J, 2018,345:196-208.

[34] Liu Z, Fan W, Xue Z, et al. Diffusion of n-alkanes in mesoporous 5A zeolites by ZLC method[J]. Adsorption, 2013,19(1):201-208.

[35] Hufton J R, Ruthven D M. Diffusion of light alkanes in silicalite studied by the zero-length column method[J]. Ind Eng Chem Res, 1993,32(10):2379-2386.

[36] Mears D E. Tests for transport limitations in experimental catalytic reactors[J]. Ind Eng Chem Process Des Dev, 1971,10(4):541-547.

[37] Banu I, Bumbac G, Bombos D, et al. Glycerol acetylation with acetic acid over Purolite CT-275. Product yields and process kinetics[J]. Renew Energ, 2020,148:548-557.

[38] Zhao Y, Guo Z, Zhang H, et al. Hydrogenation of diesters on copper catalyst anchored on ordered hierarchical porous silica: Pore size effect[J]. J Catal, 2018,357:223-237.

[39] Satterfield C. The role of diffusion in catalysis[M]. Addison-Wesley Pub. Co., 1964.

[40] Tsai M C, Chen Y W, Li C. Restrictive diffusion under hydrotreating reactions of heavy residue oils in a trickle bed reactor[J]. Ind Eng Chem Res, 1993,32(8):1603-1609.

[41] Gang W, Chen Z, Lan X, et al. Restricted diffusion of residual molecules in catalyst pores under reactive conditions[J]. Chem Eng Sci, 2011,66(6):1200-1211.

[42] Chantong A, Massoth F E. Restrictive diffusion in aluminas[J]. AIChE J, 1983,29(5):725-731.

[43] Yakimchenko O E, Degtyarev E N, Parmon V N, et al. Diffusion in porous catalyst grains as studied by EPR imaging[J]. J Phy Chem, 1995,99(7):2038-

2041.

[44] Cimenler U, Joseph B, Kuhn J N. Hydrocarbon steam reforming using silicalite-1 zeolite encapsulated Ni-based catalyst[J]. AIChE J, 2017,63(1):200-207.

[45] Mukherjee S, Vannice M A. Solvent effects in liquid-phase reactions - I. Activity and selectivity during citral hydrogenation on Pt/SiO$_2$ and evaluation of mass transfer effects[J]. J Catal, 2006,243(1):108-130.
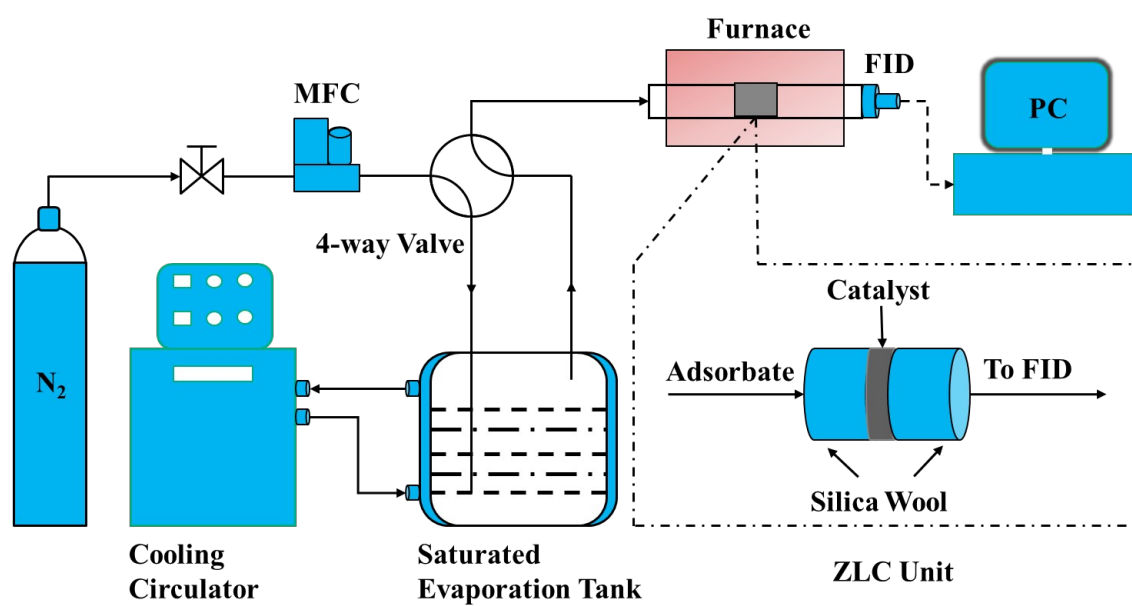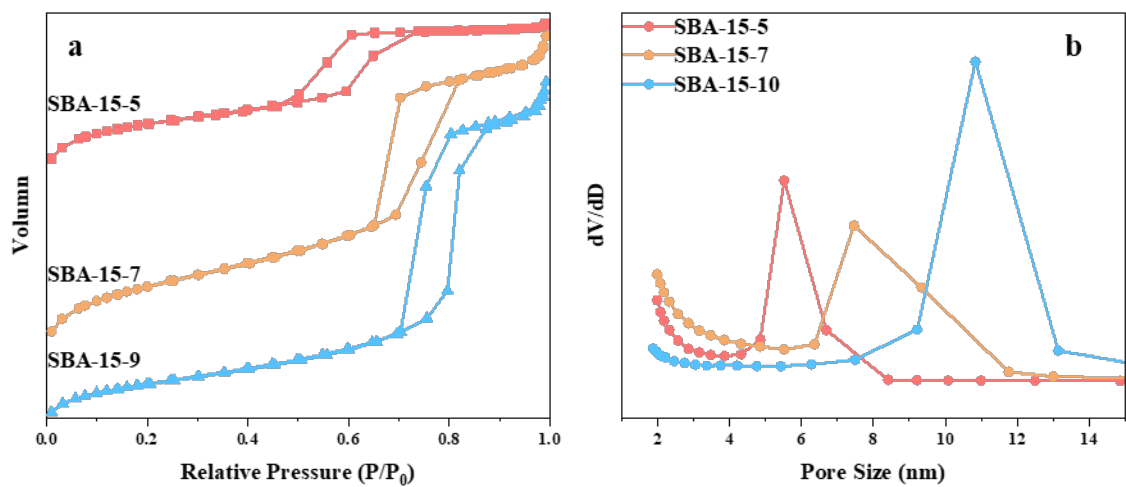
Fig. 1 Schematic diagram of the ZLC apparatus

Fig. 2 Nitrogen adsorption isotherms (a) and pore distribution curves (b) of SBA-15-n

Sample	Surface area (m^2/g)	Pore volume (cm^3/g)	Pore size (nm)
SBA-15-5	770.8	0.65	4.85
SBA-15-7	765.6	1.12	6.66
SBA-15-10	521.6	1.08	9.64

Table 1 Textural properties of SBA-15-n

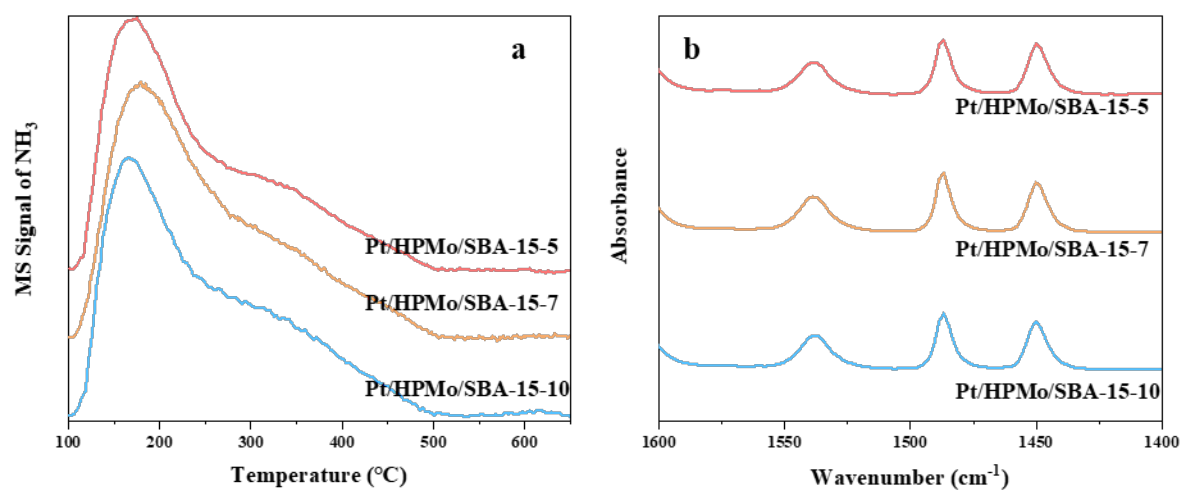**Fig. 3 XRD patterns of SBA-15-n (a) and Pt/HPMo/SBA-15-n (b)**

Fig. 4 NH$_3$-TPD curves (a) and Py-FTIR patterns (b) Pt/HPMo/SBA-15-n

Sample	B acid sites (μmol/g)	L acid sites (μmol/g)	Pt/H^{+} [a]
Pt/HPMo/SBA-15-5	296.2	231.5	0.042
Pt/HPMo/SBA-15-7	306.9	219.7	0.035
Pt/HPMo/SBA-15-10	294.4	213.9	0.041

[a] calculated based on CO-Titration measurement
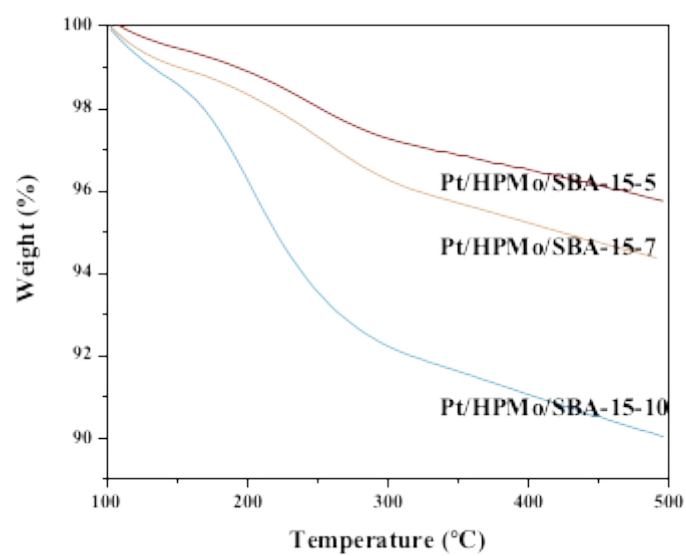
Table 2 Acidic and metallic properties of Pt/HPMo/SBA-15-n
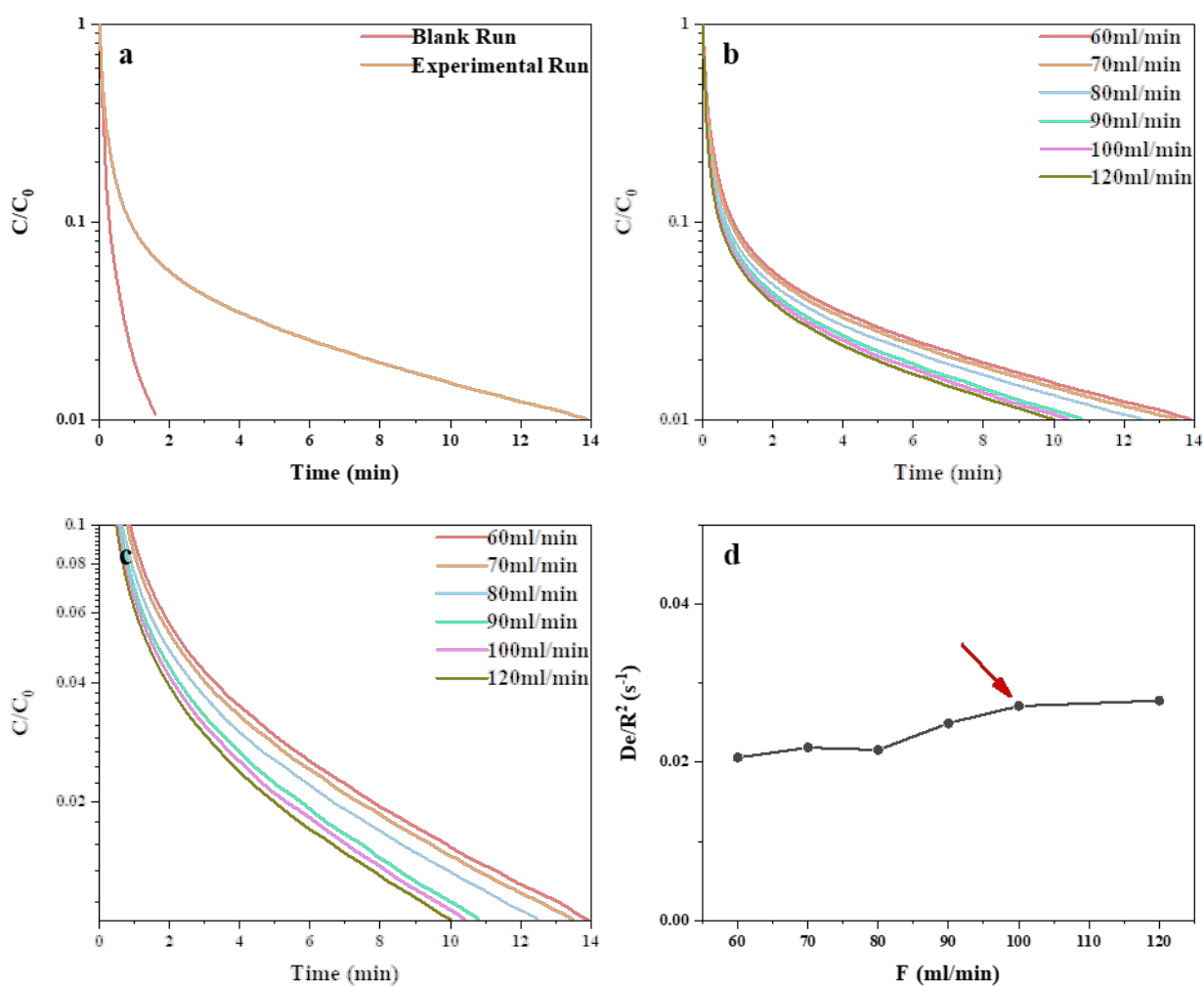
Fig. 5 TG-TPD curves of n-C16 over Pt/HPMo/SBA-15-n

Fig. 6 Experimental condition verification chart of ZLC over Pt/HPMo/SBA-15-5: Blank control plot of desorption curve (a), Desorption curves at different flows (b&c), and effective diffusion time constants at different flows (d)
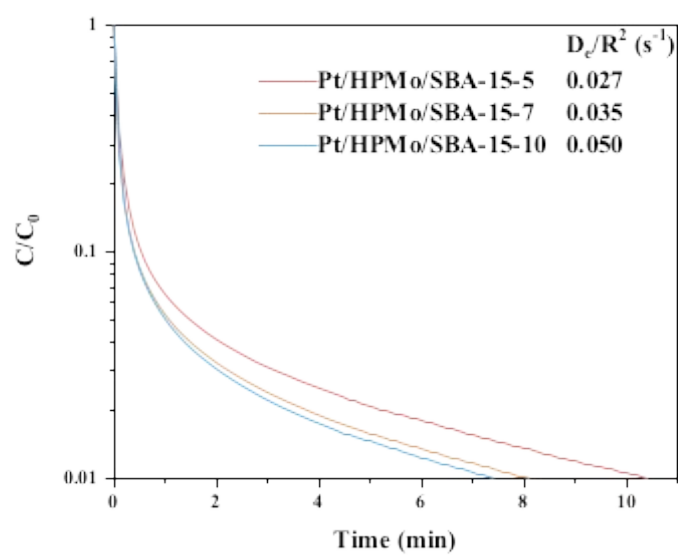
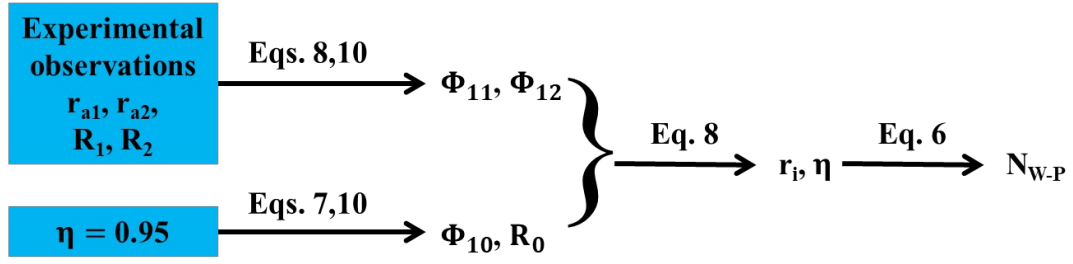**Fig. 7 Desorption curves and effective diffusion time constants of Pt/HPMo/SBA-15-n**

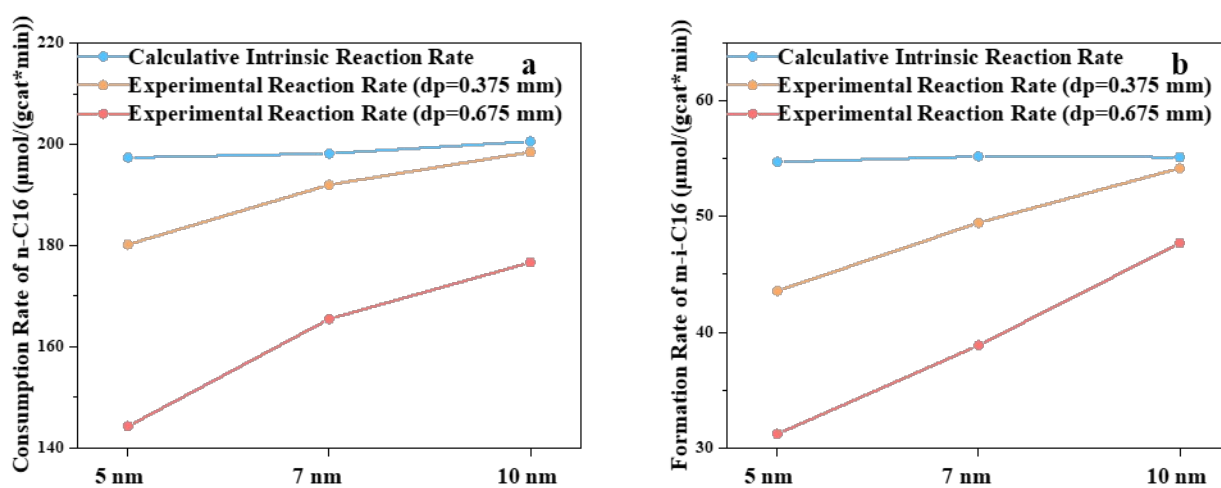**Fig. 8 Scheme of calculation in the novel method to determine N_{W-P}**

Fig. 9 Consumption rate of n-C16 (a) and formation rate of m-i-C16 (b) over Pt/HPMo/SBA-15-n

Sample	dp_0 [a] (mm)	dp_0 [b] (mm)	Weisz-Prater Number			
			dp= 0.675 mm [a]	dp= 0.375 mm [a]	dp= 0.675 mm [b]	dp= 0.375 mm [b]
Pt/HPMo/SBA-15-5	0.215	0.143	4.70	1.36	8.79	3.40
Pt/HPMo/SBA-15-7	0.290	0.200	2.69	0.48	5.39	7.65
Pt/HPMo/SBA-15-10	0.340	0.321	1.91	0.17	2.16	0.26

dp_0: theoretical value of particle diameter when the internal diffusion is virtually eliminated

a: calculated based on the consumption rate of n-C16

b: calculated based on the formation rate of m-i-C16

Table 3 Weisz-Prater Number of Pt/HPMo/SBA-15-n